Available online at www.sciencedirect.com
ScienceDirect
Trans. Nonferrous Met. Soc. China 28(2018) 282−289
Transactions of Nonferrous Metals Society of China
www.tnmsc.cn

Phase equilibria of Al−Fe−Sn ternary system

Yong-xiong LIU, Fu-cheng YIN, Jing-xian HU, Zhi LI, Si-han CHENG

Key Laboratory of Materials Design and Preparation Technology of Hunan Province,
School of Materials Science and Engineering, Xiangtan University, Xiangtan 411105, China

Received 22 September 2016; accepted 12 January 2017

Abstract: The isothermal sections of Al−Fe−Sn ternary system at 973 and 593 K were determined experimentally by the equilibriated alloy method using scanning electron microscopy coupled with energy-dispersive spectrometry and X-ray diffractometry. Experimental results show that no ternary compound is found on these two sections. The maximum solubility of Fe in the liquid phase is 1.6% (mole fraction) at 973 K and those of Fe and Al in the liquid phase are 0.6% and 5.1% (mole fraction) at 593 K, respectively. The maximum solubility of Sn in the Fe−Al compounds is 4.2% (mole fraction) at 973 K and 2.3% (mole fraction) at 593 K. All the Fe−Al compounds can be in equilibrium with the liquid phase.
Key words: Al−Fe−Sn ternary system; phase diagram; solubility

1 Introduction

In the modern manufacturing industry, combination of different materials, e.g., steel and aluminum alloy, has been widely applied in order to reduce the mass of vehicle and decrease of the fuel consumption [1,2]. Some different methods are used to produce Al/Fe cladding materials [3,4]. However, joining of the two kinds of different materials is a great challenge because of the large differences in thermo-physical properties between them and the formation of brittle intermetallic compounds at elevated temperatures [5]. Generally, some alloying elements, such as Si and Sn, are added to aluminum alloy in order to meet the challenge [6]. Knowledge of phase equilibrium in the Al−Fe−Si−Sn quaternary system is useful to fully understand the effect of Si and Sn on the joining process.

The phase relation of the Al−Fe−Si−Sn quaternary system is also important for designing the composition of bath in the hot-dip-aluminizing (HDA). HDA is a widely used anticorrosion technology which can prevent oxidation at high temperature [7,8]. However, the dramatic reaction between the molten and the steel substrate during HDA in pure Al or 55%Al−Zn bath may lead to the formation of thick and brittle interlayer Fe_2Al_5. This interlayer can be detrimental to the forming performance of the aluminized steel. Moreover, high temperature will result in severe oxidation of the aluminum bath and damage of equipment of hot dip plating operation [9]. Hence, it is important to decrease the hot-dipping temperature and reduce the thickness of the intermetallic layer by adding alloying elements in the aluminum bath. Si in bath can inhibit the Fe−Al reaction and reduce the thickness of the coating [10,11]. Sn is an important element that can increase the fluidity and reduce all the $L\rightarrow S$ transformation temperatures of the bath [12]. Therefore, the information of the phase relationships of the Al−Fe−Si−Sn quaternary system is essential to understand the synergistic effect of Sn and Si in HDA.

However, the phase diagram of the Al−Fe−Sn ternary system was determined experimentally just at room temperature in 1988 [13], and the phase relationship of the Al−Fe was not perfect in that time. Furthermore, there is no information about this ternary system at the correlative temperature in the literature.

Due to its importance, the Al−Fe binary system was investigated repeatedly [14−16]. The generally accepted Al−Fe phase diagram is from an assessment by KATTNER and BURTON [14]. But they did not present a set of parameters to calculate the whole diagram as the modeling technique at that time did not allow an acceptable thermodynamic model for the B2 and DO_3

Foundation item: Projects (51471141, 51471140) supported by the National Natural Science Foundation of China; Project (2016JC2005) supported by the Scientific Research Fund of Hunan Provincial Science and Technology Department, China
Corresponding author: Fu-cheng YIN; Tel: +86-731-58298428; E-mail: fuchengyin@xtu.edu.cn
DOI: 10.1016/S1003-6326(18)64661-8

ordering. Later, the Al−Fe binary system was assessed by SUNDMAN et al [15]. Recently, the Al-rich part of the Fe−Al phase diagram was re-investigated in detail by LI et al [16]. There are four intermetallic compounds, $FeAl_3$, Fe_2Al_5, $FeAl_2$ and FeAl in the binary Al−Fe system. All of them indicate certain homogeneities according to the literature. In the present work, it was identified by its chemical composition according to the available Al−Fe binary phase diagram.

The Fe−Sn binary system has been investigated repeatedly [17,18]. The experimental data and thermodynamic calculation of Fe−Sn phase diagram were summarized and assessed again by HUANG et al [18]. Their calculated results were in good agreement with the experimental information. There are three intermetallic compounds, Fe_3Sn_2, FeSn and $FeSn_2$, with no homogeneity. Al−Sn is a simple eutectic system with limited solid solubility in the two terminal solid solutions, FCC (Al) and tetragonal (β-Sn) [19,20]. There is no information about the Al−Fe−Sn ternary phase diagram (The available information on the crystal structures of the phases involved in the present work is summarized in Table 1). Therefore, in this work, the phase equilibria of Al−Fe−Sn ternary system at 973 and 593 K were investigated.

2 Experimental

The phase relationships of the Al−Fe−Sn ternary system are deduced by the equilibriated alloy method. The designed compositions of these alloys are listed in Tables 2 and 3. The purities of raw materials, i.e., Fe and Al powders and Sn shots, are 99.99% (mass fraction). The mixture of the raw materials, with the mass of each constituent precisely measured to an accuracy of 0.0001 g and a total mass of 5 g, was used. Because Al can react with the quartz tube at elevated temperatures, the mixture of the three elements was mixed and put into a corundum crucible which was sealed in an evacuated quartz tube. Each sample was heated to 1423 K and kept for 2 d, then quenched in water. Some quenched samples were annealed at 973 K for 40 d to detect the 973 K isothermal section. And some quenched samples were annealed at 593 K for 60 d to detect the 593 K isothermal section, to ensure the establishment of an equilibrium state. The treatment was completed with water quenching quickly to preserve the equilibrium state at annealing temperatures.

The specimens were prepared in the conventional way for metallographic examinations. A nital etching solution was used for revealing the microstructure details and a conventional optical microscope was used for the preliminary examination of all specimens. Detailed metallographic examinations and compositional analyses of various phases in the samples were performed using a JSM−6360LV scanning electron microscope (SEM) coupled with OXFORD INCA energy-dispersive spectrometry (EDS). The constituent phases were further identified by analyzing XRD patterns generated by a Rigaku Ultimate IV D/max-rA X-ray diffractometer, operating at 40 kV and 40mA with Cu K_α radiation.

3 Results

All phases found in the equilibrated alloys are listed in Table 2 for 973 K and Table 3 for 593 K (Column 3), respectively, together with the chemical compositions determined by EDS (Columns 4, 5 and 6). The reported compositions are averages at least five measurements. The β-Sn phase is in liquid state at 973 and 593 K, denoted as "*L*" herein unless otherwise noted.

3.1 Phase equilibrium of Al−Fe−Sn ternary system at 973 K

Nine equilibrated alloys with the compositions listed in Table 2 were designed to determine the 973 K isothermal section. The typical alloys with different microstructures are discussed as follows, and particular attention is paid to those located in the three-phase equilibria regions.

Table 1 Crystallographic parameters for binary compounds relevant in present work

Compound	Crystal system	Space group	Cell parameter				Reference
			a/Å	*b*/Å	*c*/Å	*β*/(°)	
$FeAl_3$	Monoclinic	$C2/m$	15.49	8.08	12.48	107.69	[21]
Fe_2Al_5	Orthorhombic	$Cmcm$	7.66	6.42	4.22		[22]
$FeAl_2$	Triclinic	$P1(1)$	4.878	6.461	8.800		[23]
FeAl	Cubic	$Pm\bar{3}m(221)$	2.889	2.889	2.889		[23]
Fe_3Sn_2	Rhombohedral	$R\bar{3}m$	5.344	5.344	19.845	120	[24]
FeSn	Hexagonal	$P6/mmm$	5.300	5.300	4.449	120	[25]
$FeSn_2$	Tetragonal	$I4/mcm$	6.539	6.539	5.325		[26]

Table 2 Alloys and phase compositions of typical alloys in Al−Fe−Sn system at 973 K

Typical alloy	Designed composition	Phase	Mole fraction/%		
			Al	Fe	Sn
A1	65Al−15Fe−20Sn	*L*	52.1	0.4	47.5
		$FeAl_3$	75.1	24.9	0
A2	60Al−20Fe−20Sn	*L*	4.2	0.7	95.1
		$FeAl_3$	75.0	24.9	0.1
		Fe_2Al_5	71.3	28.7	0
A3	55Al−25Fe−20Sn	*L*	3.3	1.1	95.6
		Fe_2Al_5	70.3	29.7	0
		$FeAl_2$	66.2	33.8	0
A4	48Al−32Fe−20Sn	*L*	2.8	1.1	96.1
		$FeAl_2$	62.9	36.8	0.3
		FeAl	48.3	51.1	0.6
A5	30Al−50Fe−20Sn	*L*	1.6	1.6	96.8
		FeAl	35.2	63.6	1.2
A6	10Al−60Fe−30Sn	*L*	1.4	1.5	97.1
		α-Fe	16.5	79.3	4.2
		FeSn	1.4	50.2	48.4
A7	6Al−64Fe−30Sn	*α*-Fe	13.5	84.2	2.3
		FeSn	0.9	50.3	48.8
A8	3Al−67Fe−30Sn	*α*-Fe	7.9	89.8	2.3
		FeSn	0	50.2	49.8
		Fe_3Sn_2	0	59.4	40.6
A9	3Al−77Fe−20Sn	*α*-Fe	6.0	92.2	1.8
		Fe_3Sn_2	0.2	61.2	38.6

Table 3 Alloys and phase compositions of typical alloys in Al−Fe−Sn system at 593 K

Typical alloy	Designed composition	Phase	Mole fraction/%		
			Al	Fe	Sn
B1	65Al−15Fe−20Sn	*α*(Al)	99.9	0	0.1
		L	5.1	0.4	94.5
		$FeAl_3$	75.3	24.6	0.1
B2	60Al−20Fe−20Sn	*L*	3.5	0.5	96.0
		$FeAl_3$	75.6	24.3	0.1
		Fe_2Al_5	72.9	27.1	0
B3	55Al−25Fe−20Sn	*L*	2.6	0.6	96.8
		Fe_2Al_5	70.1	29.6	0.3
		$FeAl_2$	66.9	31.9	1.2
B4	48Al−32Fe−20Sn	*L*	2.3	0.3	97.4
		$FeAl_2$	66.2	33.8	0
		FeAl	49.4	50.4	0.2
B5	32Al−48Fe−20Sn	*L*	2.2	0.4	97.4
		FeAl	40.1	58.7	1.2
B6	23Al−47Fe−30Sn	*L*	2.2	0.2	97.6
		FeAl	36.1	61.6	2.3
		$FeSn_2$	0.4	32.6	67.0
B7	10Al−60Fe−30Sn	*α*-Fe	18.1	80.7	1.2
		$FeSn_2$	0.4	32.7	66.9
B8	4Al−66Fe−30Sn	*α*-Fe	8.1	90.1	1.8
		FeSn	1.1	50.5	48.4
		$FeSn_2$	0.3	32.8	66.9
B9	2Al−68Fe−30Sn	*α*-Fe	2.7	96.6	0.7
		FeSn	1.2	50.7	48.1

3.2 Phase equilibrium of Al−Fe−Sn ternary system at 593 K

Nine equilibrated alloys with the compositions listed in Table 3 were designed to determine the 593K isothermal section. The typical alloys with different microstructures are discussed as follows, and particular attention is paid to those located in the three-phase equilibria regions.

4 Discussion

4.1 Phase equilibrium of Al−Fe−Sn ternary system at 973 K

Figure 1 shows the microstructures of the alloys in which there are Fe−Al compounds. The microstructure of alloy A1 is shown in Fig. 1(a). Based on the SEM−EDS analyses, this alloy consists of a black blocky $FeAl_3$ phase and primary dendrites of *α*(Al). The *α*(Al) forms from liquid phase during the water quenching process. The blocky $FeAl_3$ phase contains 75.1% Al and 24.9% Fe (mole fraction) with almost no Sn. XRD patterns shown in Fig. 2 confirm that the phase is the $FeAl_3$ phase. SEM−EDS analyses and XRD patterns indicate that it consists of a mixture of *α*(Al) and *β*-Sn. So, alloy A1 should be in the $FeAl_3$+*L* two-phase equilibria state. The composition of the *L* phase is determined by measuring the area fractions of the *β*-Sn and *α*(Al) phase dendrite using EDS. The *L* phase contains 52.1% Al, 47.5% Sn and 0.4% Fe. Figure 1(b) shows the microstructure of alloy A2. Experimental results indicate that it consists of the gray *L* phase, the black blocky $FeAl_3$ phase and the gray Fe_2Al_5 grain. The matrix *L* phase contains 4.2% Al and 0.7% Fe. And Sn is hardly detected in the $FeAl_3$ phase and Fe_2Al_5 phase. It can be seen from Fig. 1(c) that alloy A3 consists of the matrix *L* phase and the gray blocky Fe_2Al_5 phase attached around the light gray $FeAl_2$ phase. EDS analyses indicate that no Sn is detected in the $FeAl_2$ phase and Fe_2Al_5 phase. Figure 1(d) shows the microstructure of alloy A4. SEM−EDS analyses suggest that the light gray FeAl phase and the black $FeAl_2$ phase coexist with the white *L* phase in alloy A4. The *L* phase contains 2.8% Al and 1.1% Fe.

The typical XRD patterns of the four alloys A1−A4 are shown in Fig. 2. The pattern of alloy A1 indicates that it consists of mixture of *α*(Al)+*β*-Sn and $FeAl_3$ phase. The patterns of alloys A2−A4 clearly confirm the three-phase equilibria state in each alloy, respectively.

Figure 3 shows the microstructures of the alloys involving Fe−Sn compounds. Figure 3(a) shows the microstructure of alloy A6. SEM−EDS analyses indicate that three phases, i.e., gray FeSn matrix, white *L* phase and the black *α*-Fe particles co-exist in alloy A6. The *α*-Fe phase contains 16.5% Al and 4.2% Sn. The *L* phase

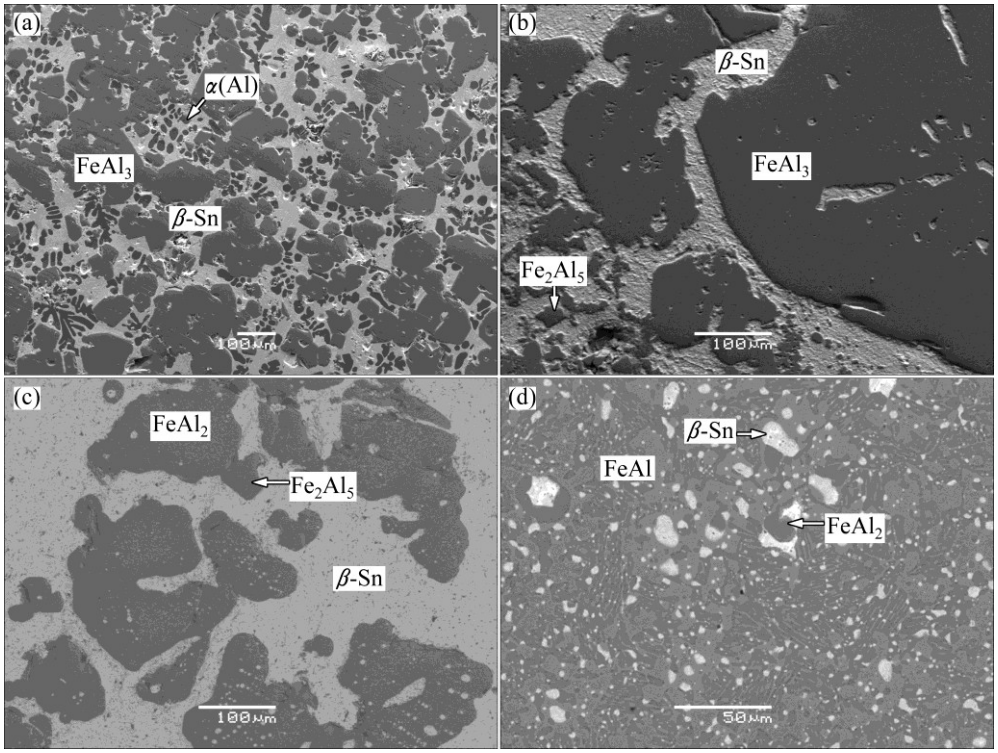

Fig. 1 Microstructures of alloy A1 (a), alloy A2 (b), alloy A3 (c) and alloy A4 (d) at 973 K

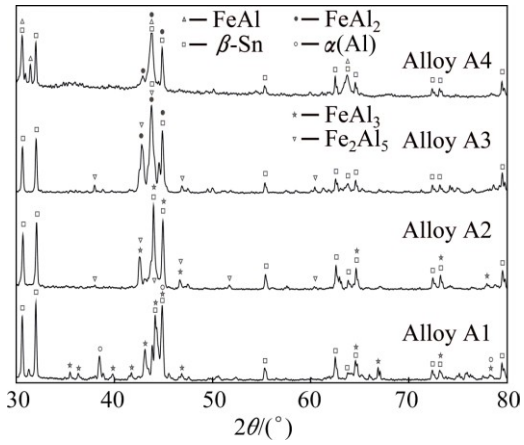

Fig. 2 XRD patterns of alloy A1, alloy A2, alloy A3, alloy A4 at 973 K

contains 1.4% Al and 1.5% Fe. The microstructure of alloy A8 is shown in Fig. 3(b). Based on the SEM−EDS analyses, this alloy consists of three phase, i.e., the gray Fe_3Sn_2 matrix which contains 59.4% Fe and 40.6% Sn, the light gray FeSn phase with 50.2% Fe and 49.8% Sn and the black strip α-Fe phase with 7.9% Al and 2.3% Sn. Fe_3Sn_2 phase and FeSn phase are not easy to distinguish. The light gray spicule which is in the α-Fe phase is FeSn. However, they are clearly differentiated from the X-ray pattern. EDS analyses suggest that no Al dissolves in Fe_3Sn_2 or FeSn. The XRD patterns of alloys A6 and A8 are shown in Fig. 3(c) which clearly indicate the three-phase equilibrium state mentioned above.

4.2 Phase equilibrium of Al−Fe−Sn ternary system at 593 K

The microstructure of alloy B1 is shown in Fig. 4(a). Based on the SEM−EDS analyses, this alloy consists of three phases, i.e., the gray blocky $FeAl_3$ phase, the black α(Al) phase and the matrix β-Sn which is transformed from the liquid phase. Fe is not dissolved in the α(Al) phase. Sn is hardly found in the $FeAl_3$ phase and the α(Al) phase. Figure 4(b) shows the microstructure of alloy B3. SEM−EDS analyses suggest that the gray matrix is the *L* phase, the black block is the $FeAl_2$ phase and the black particle is Fe_2Al_5 phase. The liquid phase contains 2.6% Al and 0.6% Fe. It can be seen from Fig. 4(c) that alloy B4 consists of the white liquid phase, the black $FeAl_2$ matrix and the gray FeAl phase. SEM−EDS analyses indicate that Sn is hardly found in the $FeAl_2$ phase and FeAl phase. The liquid phase contains 2.3% Al and 0.3% Fe. The typical XRD patterns of the three alloys B1, B3 and B4 are shown in Fig. 4(d), which clearly confirm these three-phase equilibrium states in each alloy, respectively.

The microstructure of alloy B6 is shown in Fig. 5(a). SEM−EDS analyses indicate that this alloy contains three phases, i.e., the white *L* phase, the black blocky FeAl phase and the gray blocky $FeSn_2$ phase. The FeAl phase contains 36.1% Al and 2.3% Sn. The *L* phase contains 2.2% Al and 0.2% Fe. Figure 5(b) shows the microstructure of alloy B8, which contains three phases, the dark blocky α-Fe phase, the gray blocky FeSn phase

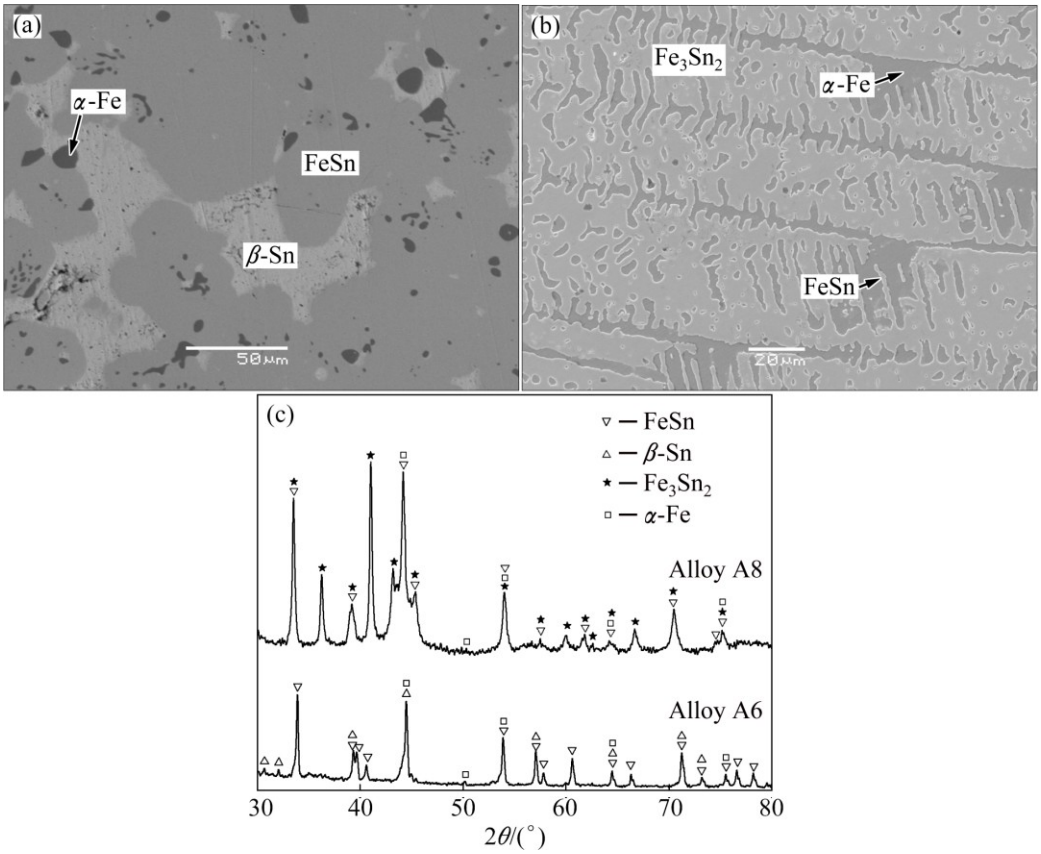

Fig. 3 Microstructures of alloy A6 (a), alloy A8 (b) and XRD patterns of two alloys (c) at 973 K

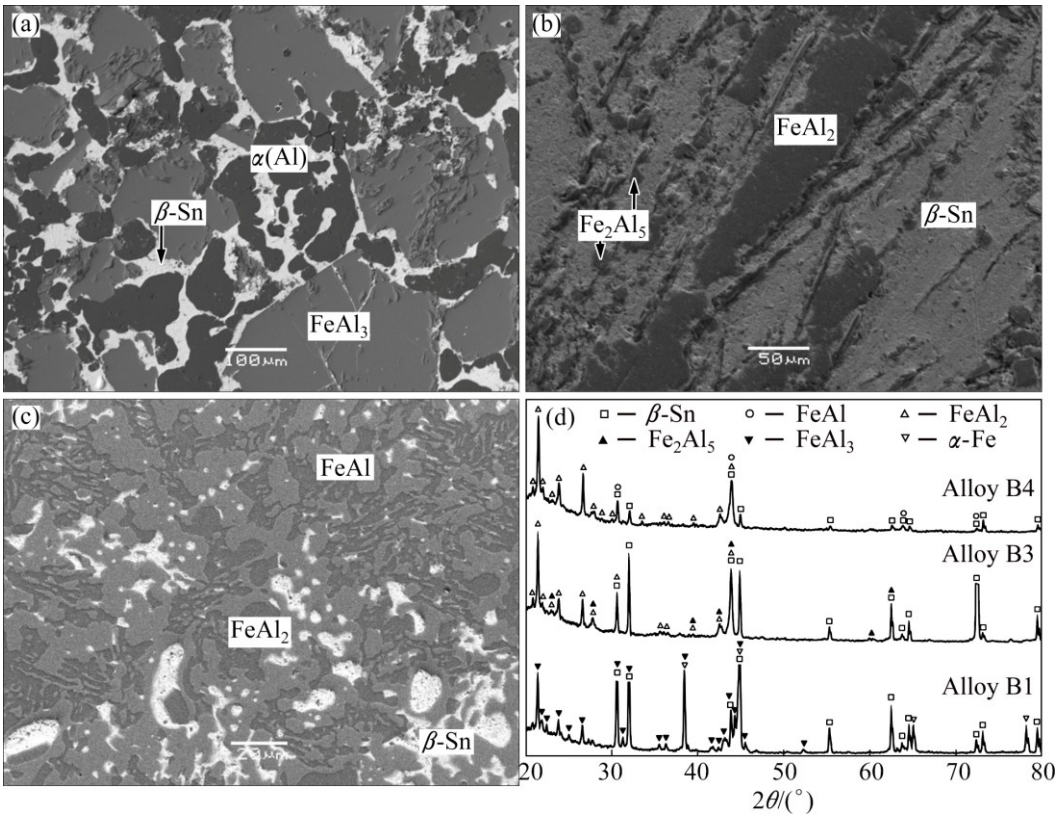

Fig. 4 Microstructures of alloy B1 (a), alloy B3 (b), alloy B4 (c) and XRD patterns of three alloys (d) at 593 K

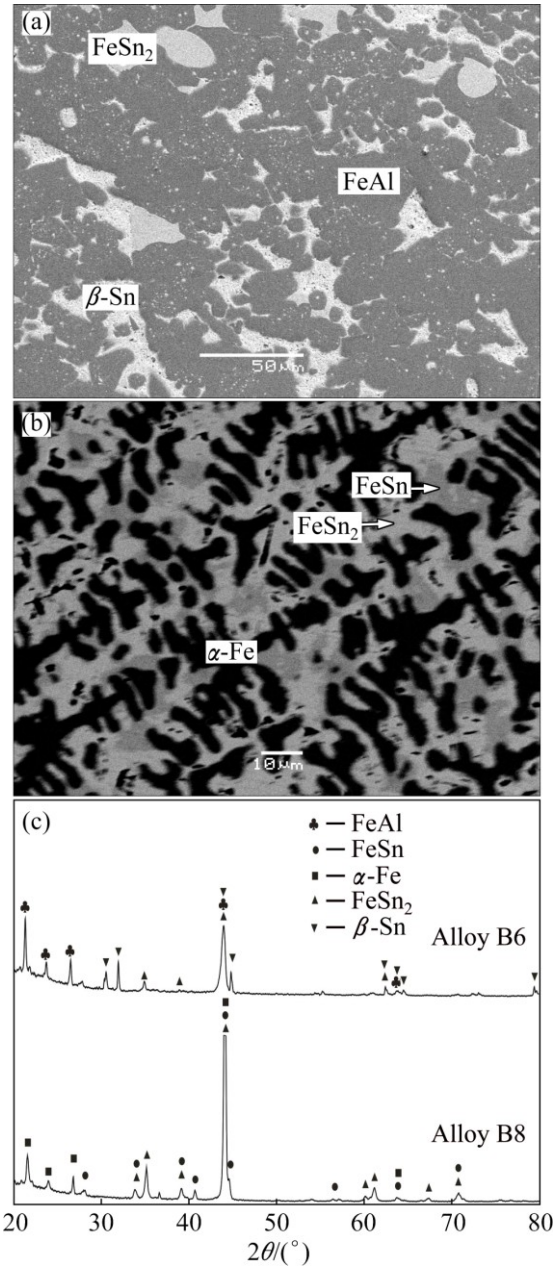

Fig. 5 Microstructures of alloy B6 (a) and alloy B8 (b) and XRD patterns of two alloys (c) at 593 K

and the white blocky $FeSn_2$ phase. The α-Fe phase contains 8.1% Al and 1.8% Sn. Figure 5(c) shows the XRD patterns of alloys B6 and B8, which clearly indicate these three-phase equilibrium states mentioned above in each alloy, respectively.

4.3 Isothermal sections of Al−Fe−Sn ternary system at 973 and 593 K

The phase diagram of the relevant binary systems is the base for the boundary of the isothermal section of the ternary system. The accepted phase diagrams of Fe−Al [14], Fe−Sn [17] and Al−Sn [19] are shown in Fig. 6.

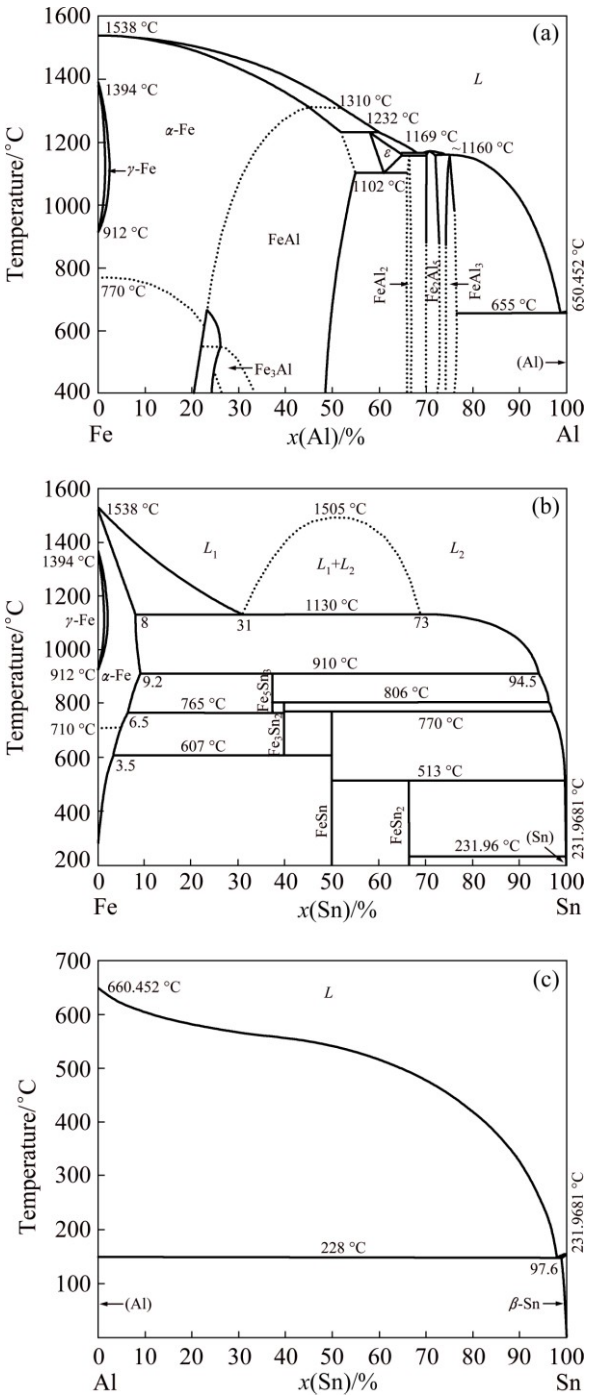

Fig. 6 Phase diagram of relevant binary systems: (a) Fe−Al [14]; (b) Fe−Sn [17]; (c) Al−Sn [19]

Based on the information of relevant binary systems and the results of microstructure observation and phase analyses, including X-ray diffraction and SEM−EDS analyses, the 973 and 593 K isothermal sections of Al−Fe−Sn ternary system are constructed and shown in Figs. 7(a) and (b), respectively.

From Fig. 7(a), it can be seen that five three-phase regions, i.e., L + $FeAl_3$ + Fe_2Al_5, L + Fe_2Al_5 + $FeAl_2$, L + $FeAl_2$ + FeAl, L + α-Fe + FeSn and α-Fe + FeSn +

Fe_3Sn_2 exist in the 973 K isothermal section. The liquid phase can be in equilibrium with the four Fe−Al intermetallic compounds. The Fe−Al intermetallic compounds contain little Sn. There is no ternary compound. The phase relationship of the 593 K isothermal section is similar to that of the 973 K section. Their difference is mostly on the Fe−Sn side. Contrasting Figs. 7(a) and (b), the equilibrium relationships around Fe_3Sn_2 or $FeSn_2$ phase are different between the two isothermal sections. On the 593 K isothermal section, the $FeSn_2$ phase is in equilibrium with FeSn and α-Fe. However, on the 973 K section, the $FeSn_2$ phase disappears and Fe_3Sn_2 phase appears. Another difference is the size of the area of liquid phase. On the 593 K isothermal section, there is a little area of liquid phase at the Sn-rich corner; however, there is a lathy area of liquid phase beside the Al−Sn side on the 973 K section.

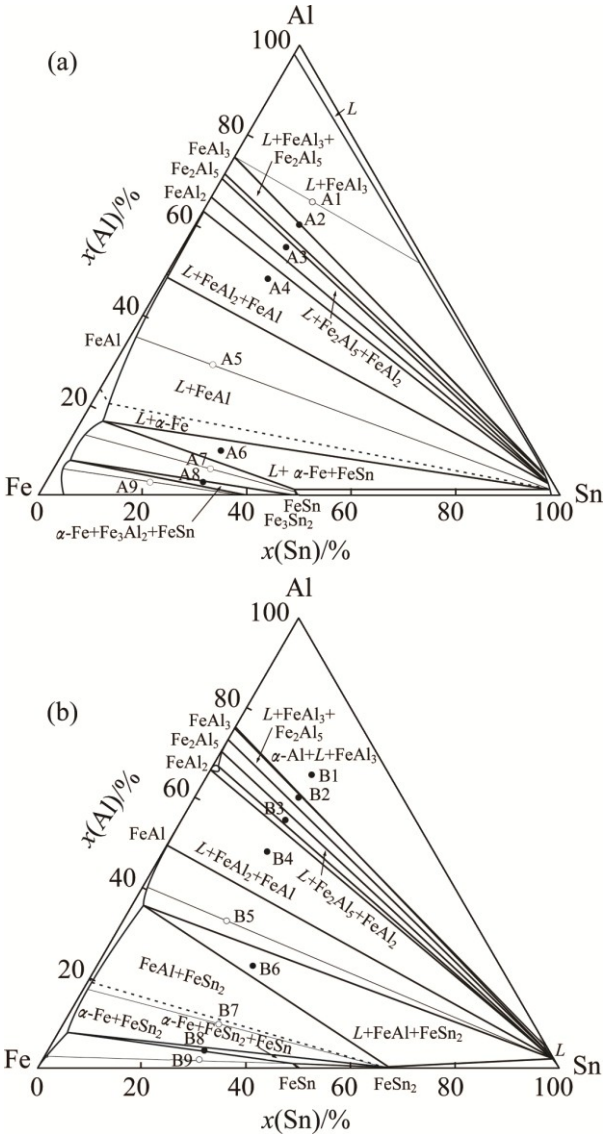

Fig. 7 Isothermal sections of Al−Fe−Sn ternary system at 973 K (a) and 593 K (b)

5 Conclusions

1) Based on SEM−EDS analyses and X-ray diffraction results, the 973 and 593 K isothermal sections of the Al−Fe−Sn ternary system are determined.

2) Five three-phase regions exist on the isothermal section at 973 K and six on the 593 K section. No ternary compound is found in this system on the two sections.

3) The liquid phase can be in equilibrium with four Fe−Al intermetallic compounds at 973 and 593 K.

4) The maximum solubilities of Fe and Al in the liquid phase are 0.6% and 5.1% (mole fraction) at 593 K, respectively, and that of Fe reaches 1.6% (mole fraction) at 973 K. The maximum solubility of Sn in the Fe−Al compounds is 4.2% (mole fraction) at 973 K and 2.3% (mole fraction) at 593 K.

References

[1] GOULD J E. Joining aluminum sheet in the automotive industry—A 30 year history[J]. Weld J, 2012, 91: 23−34.

[2] WANG Qian, LENG Xue-song, YANG Tian-hao, YAN Jiu-chun. Effects of Fe−Al intermetallic compounds on interfacial bonding of clad materials [J]. Transactions of Nonferrous Metals Society of China, 2014, 24: 279−284.

[3] ZHU Xiao-lin, YAO Zheng-jun, GU Xue-dong, CONG Wei, ZHANG Ping-ze. Microstructure and corrosion resistance of Fe−Al intermetallic coating on 45 steel synthesized by double glow plasma surface alloying technology [J]. Transactions of Nonferrous Metals Society of China, 2009, 19: 143−148.

[4] LEE J H, KIM J D, OH J S, PARK S J. Effect of Al coating conditions on laser weld ability of Al coated steel sheet [J]. Transactions of Nonferrous Metals Society of China, 2009, 19: 946−951.

[5] CHEN H C, PINKERTON A J, LI L, LIU Z, MISTRY A T. Gap-free fibre laser welding of Zn-coated steel on Al alloy for light-weight automotive applications [J]. Mater Des, 2011, 32: 495−504.

[6] SONG Jian-ling, LIN San-bao, YANG Chun-li, MA Guang-chao. Research on alloy agent for improving welded joint properties of Aluminum to steel dissimilar material [J]. Aeronautical Manufacturing, 2008, 12: 26−28. (in Chinese)

[7] GEORGE Y L. High-temperature corrosion of engineering alloys [M]. Ohio: ASM International, 1990.

[8] LANG E. Coatings for high temperature applications [M]. New York: Applied Science Publishers, 1984.

[9] XIAO Gang, SHANGGUAN Qi, LU Yu-heng, HUANG Cai-ming, and ZENG Jian-min. Heat transfer during the solidification of hot dip aluminizing coating [J]. Chinese Journal of Mechanical Engineering, 2011, 24(3): 460−465. (in Chinese)

[10] YIN Fu-cheng, ZHAO Man-xiu, LIU Yong-xiong, HAN Wei, LI Zhi. Effect of Si on the growth kinetics of intermetallic compounds during the reaction of solid iron and molten aluminum [J]. Transactions of Nonferrous Metals Society of China, 2013, 23: 556−561.

[11] HAN S L, LI H L, WANG S M, JIANG L J, LIU X P. Influence of silicon on hot-dip aluminizing process and subsequent oxidation for preparing hydrogen/tritium permeation barrier [J]. International Journal of Hydrogen Energy, 2010, 35(7): 2689−2693.

[12] KLIAUGA A M, FERRANTE M. The effect of Sn additions on the semi-solid microstructure of an Al−7Si−0.3Mg alloy [J]. Materials Science and Engineering A, 2002, 337: 67−72.
[13] CHEN R Z, LU H, ZHENG J X. A phase diagram of the Al−Fe−Sn ternary system [J]. Journal of Guangxi University, 1988, 2: 62−64. (in Chinese)
[14] KATTNER U R, BURTON B P. Al−Fe(aluminum−iron): Phase diagrams of binary iron alloys [M]. Ohio: ASM International, 1993.
[15] SUNDMAN B, OHNUMA I, DUPIN N, URSULA R K, SUZANA G F. An assessment of the entire Al−Fe system including DO_3 ordering [J]. Acta Materialia, 2009, 57(10): 2896−2908.
[16] LI Xiao-lin, SCHERF A, HEILMAIER M, STEIN F. The Al-rich part of the Fe−Al phase diagram [J]. Journal of Phase Equilibria and Diffusion, 2016, 37(2): 162−173.
[17] MASSALSKI T B, OKAMOTO H, SUBRAMANIAN P R, KACPRZAK L. Binary alloy phase diagrams [M]. 2nd ed. Ohio: ASM International, 1990.
[18] HUANG Y C, GIERLOTKA W, CHWN S W. Sn−Bi−Fe thermodynamic modeling and Sn−Bi/Fe interfacial reactions [J]. Intermetallics, 2010, 18: 984−991.
[19] MCALISTER A J, KAHAN D J. The Al−Sn (aluminum−tin) system [J]. Bulletin of Alloy Phase Diagrams, 1983, 4(4): 410−414.
[20] FRANKE P, NEUSCHUTZ D. Binary systems part 5: Binary systems supplement 1 [M]. Aachen: Landolt−Börnstein−Group IV Physical Chemistry: Scientific Group Thermodata Europe (SGTE), 2007.
[21] GRIN J, BURKHARDT U, ELLNER M. Refinement of the Fe_4Al_{13} structure and its relationship to the homological homeotypical structures [J]. Crystalline Materials, 1994, 209(6): 479−487.
[22] BURKHARDT U, GRIN Y, ELLNER M. Structure refinement of the iron−aluminium phase with the approximate composition Fe_2Al_5 [J]. Acta Crystallographica Section B: Structural Science, 1994, 50(3): 313−316.
[23] MASSALSKI T B. Binary alloy phases diagrams [M]. Ohio: ASM International, 1986.
[24] MALAMAN B, ROQUES B, COURTOIS A, PROTAS J. Crystal structure of the Fe_3Sn_2 [J]. Acta Crystallogr B, 1976, 32: 1348−1351.
[25] van der KRAAN A M, BUSCHOW K H J. The ^{57}Fe Mössbauer isomer shift intermetallic compounds of iron [J]. Physica B, 1986, 138(1−2): 55−62.
[26] CAER G L, MALAMAN B, VENTURINI G, FRUCHART D, ROQUES B. A Mossbauer study of $FeSn_2$ [J]. Journal of Physics F: Metal Physics, 1985, 15: 1813−1827.

Al−Fe−Sn 三元体系的相平衡

刘永雄，尹付成，胡静娴，李 智，成思翰

湘潭大学 材料科学与工程学院 材料设计及制备技术湖南省重点实验室，湘潭 411105

摘 要：利用平衡合金法，采用扫描电镜−能谱仪和 X 射线衍射方法对 Al−Fe−Sn 三元系 973 和 593 K 等温截面的相关系进行实验测定。实验结果表明：在此两个截面上均未检测到三元化合物；973 K 时液相中 Fe 的最大固溶度为 1.6% (摩尔分数)，而 593 K 时 Fe 和 Al 在液相中的最大固溶度分别为 0.6%和 5.1% (摩尔分数)；在 973 和 593 K 等温截面上，Sn 在 Fe−Al 化合物中的最大固溶度分别为 4.2%和 2.3% (摩尔分数)；Fe−Al 化合物均能与液相保持平衡。

关键词：Al−Fe−Sn 三元系；相图；固溶度

(Edited by Wei-ping CHEN)